Available online at www.sciencedirect.com
ScienceDirect
Acta Materialia 55 (2007) 1947–1953
Acta MATERIALIA
www.actamat-journals.com

A general shape/size-effect law for nanoindentation

Nicola M. Pugno

Department of Structural Engineering, Politecnico di Torino, Corso Duca degli Abruzzi 24, Torino 10129, Italy

Received 26 June 2006; received in revised form 26 September 2006; accepted 28 October 2006
Available online 10 January 2007

Abstract

In this paper we derive a general scaling law for nanoindentation, considering different sizes and shapes of the indenter. The law matches as limit cases all the well-known hardness scaling laws proposed in the literature. But our findings, based only on the surface-to-volume ratio of the domain in which the energy flux occurs, can also explain the deviations experimentally observed at the nanoscale. Finally, a general spatial–temporal scaling law is formulated and examples of applications in different fields, such as materials science and biology, are provided.

Keywords: Hardness; Dislocation; Nanostructure; Scaling

1. Introduction

Hardness is defined as the load divided by the projected area of the indentation, thus it is the mean pressure that a material will support under load. This parameter is only "nominally" a constant and is experimentally dependent on penetration depth and size and shape of the indenter. A variation in hardness versus penetration depth is usually defined, perhaps not properly, as the indentation size-effect, whereas we refer, in this paper, to the variation of hardness by varying the size or shape of the indenter as the true size- or shape-effect, respectively.

Much of the early work on indentation has been reviewed by Mott [1]. Ashby [2] proposed that geometrically necessary dislocations [3] would lead to an increase in hardness measured by a flat punch. The problem of a conical indenter has recently been investigated [4], showing a consistent agreement with micro-indentation experiments. However, recent results that cover a greater range of depths show only partial [5,6] or no agreement [7] with this model [4]. Thus, Swadener et al. [6] extended this work in a very interesting way, to treat indenters of different sizes and shapes; the results were compared with micro-indentation experiments, but limitations for small depths of pyramidal indenters or sizes of spherical indenters were observed, as pointed out by the same authors.

The aim of this paper is the development of a new model capable of matching as limit cases the discussed indentation laws, simultaneously capturing the deviation observed towards the nanoscale. Moreover, a general spatial–temporal scaling law is formulated, that could reveal interesting applications in different fields, e.g., for complex and chaotic biosystems.

2. A general shape/size-effect law for nanoindentation

Consider an indenter with a given geometry $h = h(r, \vartheta)$, with r and ϑ being polar coordinates. Previous models [4,6] assume that plastic deformation of the surface is accompanied by the generation of geometrically necessary dislocation loops, in the treatment of length $l(h)$, below the surface; the deformation volume is assumed to be a hemispherical zone below the (projected) contact area A with radius $a = \sqrt{A/\pi}$ or volume (Fig. 1)

$$V = 2\pi/3(A/\pi)^{3/2}. \tag{1}$$

Thus, the total length L of the geometrically necessary dislocation loops can be evaluated by summating the number of steps on the staircase-like indented surface (see Fig. 1)

E-mail address: nicola.pugno@polito.it

1359-6454/$30.00
doi:10.1016/j.actamat.2006.10.053

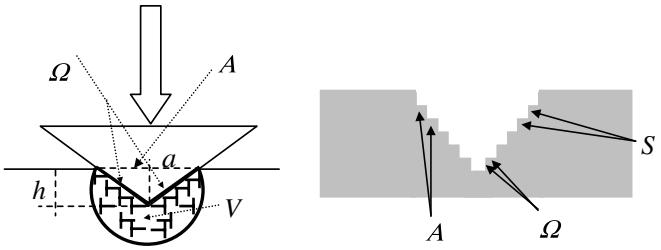

Fig. 1. Geometrical necessary dislocations during indentation: h is the indentation depth, a is the radius of the projected contact area A, Ω is the contact surface and V is the dissipation domain (proportional to a^3). Note that the indented surface at the nanoscale appears in discrete steps due to the formation of dislocation loops, i.e., of quantized plasticity. In our model the scaling law is predicted to be a function only of S/V, where $S = \Omega - A$.

$$L = \sum_{\text{steps}} l_i = \frac{\Omega - A}{b} = \frac{S}{b} \approx \frac{1}{b}\int_0^h l(h)\,\mathrm{d}h \tag{2}$$

where Ω is the total lateral surface area of the indented zone and b is the (modulus of the) Burger's vector. Ω is the sum of the "vertical" surfaces, S, and of the "horizontal" surfaces, A (Fig. 1). Thus, the surface S can be interpreted as the total one along with the energy flux arising, positive if outgoing (Ω) and negative if incoming (A), in the indenter. Note the generality of the result in Eq. (2), that does not need specification of the form of h, as is usually required.

Accordingly, the average geometrically necessary dislocation density is

$$\rho_{\mathrm{G}} = \frac{L}{V} = \frac{S}{bV}. \tag{3}$$

The actual number of dislocations that must be generated to accommodate plastic deformation, that we could call geometrically "sufficient" dislocations, is greater than the number of geometrically necessary dislocations [8] by the so-called Nye factor $\bar{r}$ ($\sim$2 [6]); thus, the total dislocation density is usually assumed to be $\rho_{\mathrm{T}} = \bar{r}\rho_{\mathrm{G}} + \rho_{\mathrm{S}}$, where ρ_{S} is the statistically stored dislocation density [4]. However, we note here that, according to this common formulation, $\rho_{\mathrm{T}}(V/(bS) \to 0) \to \infty$, i.e., the total dislocation density at the nanoscale diverges, whereas it must physically present a finite upper bound, that we call $\rho_{\mathrm{T}}^{(\mathrm{nano})}$. The existence of such an upper bound has very recently been confirmed [9].

Note that ρ_{T} is related to the shear strength τ_{p} by Taylor's hardening model [10], i.e.,

$$\tau_{\mathrm{p}} = \alpha\mu b\sqrt{\rho_{\mathrm{T}}} \tag{4}$$

where μ is the shear modulus and the geometrical constant α is usually in the range 0.3–0.6 for fcc metals [11]. Thus, the upper-bound $\rho_{\mathrm{T}}^{(\mathrm{nano})}$ is related to the existence of a finite nanoscale material strength $\tau_{\mathrm{p}}^{(\mathrm{nano})}$, that is only expected to be of the order of magnitude of the theoretical material strength at the true atomic scale.

Accordingly, the upper bound $\rho_{\mathrm{T}}^{(\mathrm{nano})}$ is straightforwardly introduced in our model through the following asymptotic matching:

$$\frac{1}{\rho_{\mathrm{T}}} = \frac{1}{\bar{r}\rho_{\mathrm{G}} + \rho_{\mathrm{S}}} + \frac{1}{\rho_{\mathrm{T}}^{(\mathrm{nano})}}. \tag{5}$$

Note that at the atomic scale, as a consequence of the quantized nature of matter, $\rho_{\mathrm{T}}^{(\mathrm{nano})}$ must be (at least theoretically) of the order of b^{-2}, as for a pure single dislocation. This is also reflected in the fact that $\beta = 1/(b^2\rho_{\mathrm{T}}^{(\mathrm{nano})}) = (\alpha\mu/\tau_{\mathrm{p}}^{(\mathrm{nano})})^2$ is of the order of the unity, since $\alpha\mu$ is of the same order of magnitude as the theoretical material strength. Note the analogy with quantized fracture mechanics [12], that quantizing the crack advancement, as must (particularly) be at the nanoscale, predicts a finite theoretical material strength, in contrast to the result of continuum-based linear elastic fracture mechanics [13].

The flow stress is related to the shear strength by von Mises' rule, i.e., $\sigma_{\mathrm{p}} = \sqrt{3}\tau_{\mathrm{p}}$, and the hardness to flow stress by a Tabor's factor [14] of 3 [4,6], i.e., $H = 3\sigma_{\mathrm{p}}$; thus $H = 3\sqrt{3}\tau_{\mathrm{p}}$. Introducing into the previous equation the shear strength given by Eq. (4), after having substituted the total and geometrical necessary dislocation densities according to Eqs. (5) and (3), respectively, we derive

$$H = 3\sqrt{3}\alpha\mu b\{(\bar{r}S/(bV) + \rho_{\mathrm{S}})^{-1} + (\rho_{\mathrm{T}}^{(\mathrm{nano})})^{-1}\}^{-1/2}.$$

Finally, rearranging such a finding and introducing dimensionless parameters, we deduce the following hardness scaling:

$$\frac{H(S/V)}{H_{\mathrm{nano}}} = \left(\frac{\delta^2 - 1}{\ell S/V + 1} + 1\right)^{-1/2},$$
$$\frac{H(S/V)}{H_{\mathrm{macro}}} = \left(\frac{\delta^2 - 1}{\delta^2 V/(\ell S) + 1} + 1\right)^{1/2}, \quad \delta = \frac{H_{\mathrm{nano}}}{H_{\mathrm{macro}}} \tag{6}$$

with

$$H_{\mathrm{nano}} \equiv H(\ell S/V \to \infty) = 3\sqrt{3/\beta}\alpha\mu,$$
$$H_{\mathrm{macro}} \equiv H(\ell S/V \to 0) = \frac{3\sqrt{3}\alpha\mu b}{\sqrt{\rho_{\mathrm{S}}^{-1} + \beta b^2}} \text{ and } \ell = \frac{\bar{r}}{\rho_{\mathrm{S}} b},$$

i.e., a characteristic length governing the transition from the nano- to the macro-scale. From a physical point of view, note that $\ell S/V = \bar{r}\rho_{\mathrm{G}}/\rho_{\mathrm{S}}$, i.e., it is equal to the ratio of the geometrically "sufficient" and statistical stored dislocation densities, whereas $\delta = \sqrt{1 + \rho_{\mathrm{T}}^{(\mathrm{nano})}/\rho_{\mathrm{S}}}$. The two equivalent expressions in Eq. (6) correspond to a bottom-up or a top-down view, even if the bottom-up law is perhaps more physical. Eq. (6) is a general shape/size-effect law for nanoindentation, that provides the hardness as a function only of the ratio between the net surface throughout which the energy flux propagates and the volume where the energy is dissipated; or, simply stated, as a function of the surface-to-volume ratio of the domain in which the energy dissipation occurs.

As in the previously mentioned references [4,6], our model is mainly based on three rather strong, even if reasonable, assumptions: (i) the plastically deformed volume is proportional to the contact area to the power 3/2;

(ii) classical Taylor's hardening (describing the situation underneath the indenter) is valid; and (iii) the density of statistically stored dislocations does not depend on the indentation depth. We note that the law of Eq. (6) is formally not affected by assumption (i), that will, however, impose the methodology of calculating the volume V, modifying Eq. (1). In particular, the power 3/2 allows us to consider V/S as a characteristic length of the indentation process (indentation depth, indenter size or their combination with the physical dimension of a length; see the cases of the conical, parabolic or flat indenter, respectively, considered in the following section), whereas a power different from 3/2, let say $3/2+\varepsilon 1$, would imply considering V/S as the characteristic length raised to the power $1+2\varepsilon 1$. Thus, the trend predicted by the law of Eq. (6) would remain valid, but with a slightly different transition from the nano- to the macro-scale. A critical inversion would be expected in the trend only for unreasonable values of $\varepsilon 1 < -1/2$. Assumption (ii), i.e., $\tau_p \propto \rho_T^{1/2}$, could be released assuming $\tau_p \propto \rho_T^{1/2+\varepsilon 2}$; accordingly, the corresponding powers of 1/2 appearing in the bottom-up and top-down equivalent laws of Eq. (6) would become $1/2+\varepsilon 2$, modifying the maximum slope of the scaling. Releasing the third hypothesis (iii) ($\rho_S \propto (V/S)^0$), i.e., assuming $\rho_S \propto (V/S)^{\varepsilon 3}$ (for V/S describing the indentation depth, e.g., as for the conical indenter considered in the following section), would mean that Eq. (6) would have to be modified according to $lS/V \propto (S/V)^{1+\varepsilon 3}$ (similarly to the removal of assumption (i), for $2\varepsilon 1 = \varepsilon 3$) and $H_{macro} = H_{nano} \equiv 3\sqrt{3/\beta}\alpha\mu$ for $\varepsilon 3 > 0$ (no size-/shape-effects), or $H_{macro} = 0$ for $\varepsilon 3 < 0$ (vanishing macro-hardness).

Thus, our law could present modifications; however, we note that small values of $\varepsilon 1$, 2, 3 are not easily observable. Furthermore, experiments as well as intuition seem to suggest us that $\varepsilon 3 = 0$, whereas from a practical point of view $\varepsilon 1$ and $\varepsilon 2$ can be considered negligible, at least until further experimental work demonstrates otherwise.

The law of Eq. (6) can be applied in a very simple way to treat any interesting indenter geometry. However, to make a comparison it is necessary to focus on the axially symmetric profiles, i.e., $h = h(r)$, previously investigated [6].

3. Different size and shape of the indenters

3.1. Conical indenter

Consider a conical indenter with corner angle φ, $h(r) = \tan((\pi-\varphi)/2)r$; by integration (Eq. (2)) we found

$$S/V = \frac{3\tan^2((\pi-\phi)/2)}{2h},$$

that introduced into Eq. (6) gives

$$H_{cone}(h,\varphi) = H_{macro}\sqrt{1+\frac{\delta^2-1}{\delta^2 h/h^*(\varphi)+1}},$$
$$h^*(\varphi) = 3/2\ell\tan^2((\pi-\varphi)/2). \quad (7)$$

For $h/h^* \to 0$ or $\varphi \to 0, H_{cone} \to H_{nano}$, whereas for $h/h^* \to \infty$ or $\varphi \to \pi, H_{cone} \to H_{macro}$; only for the case of $\delta \to \infty, H_{cone} = H_{macro}\sqrt{1+h^*/h}$ as derived in [4] (with the identical expression for $h^*(\varphi)$). Note that such a scaling law was previously proposed by Carpinteri [15] for material strength (with h structural size). The comparison here, however, is not very significant, since the "h-size effect" is not a true size effect.

We have here derived S by integration (of l), according to Eq. (2) and for consistency with Ref. [6]. A more direct calculation considers the difference between the lateral (Ω) and base (A) surface areas (see Eq. (2)), leading to a slightly different value of h^* ($h^*(\varphi) = 3/2\ell\tan^2((\pi-\varphi)/2)(1/\sin((\pi-\varphi)/2) - 1/\tan((\pi-\varphi)/2))$) with respect to the previously calculated value ($h^*(\varphi) = 3/2\ell\tan^2((\pi-\varphi)/2)$). The ratios $h^*(\varphi)/\ell$ evaluated with the two different procedures are compared in Fig. 2 for the conical indenter: the related difference is moderate and unessential in this context, thus we conclude that both the methodologies can be applied to fit experiments.

3.2. Parabolic (spherical) indenter

Consider the case of a parabolic indenter with radius at tip R, i.e., $h = r^2/(2R)$, that for not too large an indentation depth corresponds also to the case of a spherical indenter; by integration we found $S/V = 1/R$, that introduced into Eq. (6) gives

$$H_{parabola}(R) = H_{macro}\sqrt{1+\frac{\delta^2-1}{\delta^2 R/R^*+1}}, \quad R^* = \ell. \quad (8)$$

Thus, the hardness is here not a function of the indentation depth h. For $R/R^* \to 0$, $H_{parabola} = H_{nano}$, whereas for $R/R^* \to \infty$, $H_{parabola} = H_{macro}$; only for the case of

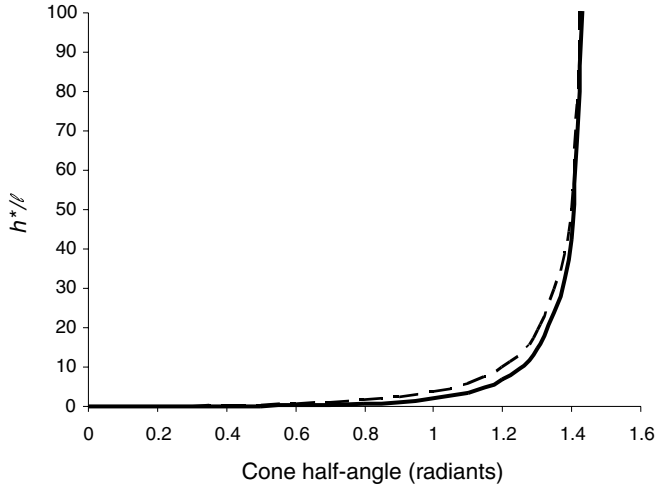

Fig. 2. Comparison for the conical indenter between the two different expressions of $h^*(\varphi)/\ell$ resulting from the two different calculation procedures for S described by Eq. (2): S directly computed as $\Omega - A$, (dashed line) or S computed by integration (solid line). Only a moderate and non-essential discrepancy is observed.

$\delta \to \infty$, $H_{\text{parabola}} = H_{\text{macro}}\sqrt{1 + R^*/R}$, as derived in Ref. [6] (with the identical expression for R^*). This law describes a true size effect and agrees with Carpinteri's law [15].

3.3. Flat indenter

Consider the case of a flat indenter of radius a, i.e., $h = \delta(r - a)$; geometrically, we found

$$S/V = \frac{2\pi a h}{2/3\pi a^3},$$

that introduced into Eq. (6) gives

$$H_{\text{flat}}(a,h) = H_{\text{macro}}\sqrt{1 + \frac{\delta^2 - 1}{\delta^2 a^2/(3h\ell) + 1}}. \tag{9}$$

For $a/\ell \to 0, H_{\text{flat}} \to H_{\text{nano}}$, whereas for $a/\ell \to \infty$, $H_{\text{flat}} \to H_{\text{macro}}$; interestingly, for $h/\ell \to 0$, $H_{\text{flat}} \to H_{\text{macro}}$, whereas for $h/\ell \to \infty$, $H_{\text{flat}} \to H_{\text{nano}}$, showing an inverse h-size effect, in agreement with the discussion by Swadener et al. [6] and with intuition (the contact area does not change when the penetration load or depth increases), see Ref. [2]. This suggests a new and intriguing methodology for the derivation of the nanoscale hardness of materials by a macroscopic experiment, using large flat punches, even if the finite curvature at the corners is expected to affect the results. This case was only discussed in Ref. [6] due to the complexity in their formalism for treating such a cuspidal geometry. Note that for $h \propto a$ and $\delta \to \infty$, the size-effect law again coincides with that of Carpinteri [15].

3.4. Experimental assessment

Swadener et al. [6] compared their model with experiments in annealed iridium, using spherical indenters of different radii ($R \approx 14, 69, 122, 318, 1600$ μm). Data were analyzed using the method of Oliver and Pharr [16]. These authors [6] treated the spherical indentation with their law for parabolic indenters, since the experiments were performed at a small value of penetration ($a/R \approx 0.05$). A hardness overestimation for $R < 80$ μm was experimentally observed. This deviation is in agreement with the prediction of Eq. (6). In particular, Swadener et al. [6] considered two plausible sets of parameters for describing their experiments (see Ref. [6] for details): (a) $H_{\text{macro}} \approx 0.9$ GPa, $R^* \approx 250$ μm or (b) $H_{\text{macro}} \approx 0.6$ GPa, $R^* \approx 750$ μm. Introducing such values into our model with, in addition, (a) $H_{\text{nano}} \approx 3$ GPa or (b) $H_{\text{nano}} \approx 5$ GPa results in a closer agreement between theory and experiment, as shown in Fig. 3a and b, respectively. Similar results with the same sets of parameters were observed for a pyramidal indenter (Berkovich, treated as a conic; from its geometry $R^*/h^* \approx 5.2$, [6]) on the same material, by varying the indentation depth. Annealed oxygen-free copper tested with spherical, Berkovich and Vickers (pyramidal, $R^*/h^* \approx 5.2$) indenters resulted in $H_{\text{macro}} \approx 0.1$ GPa and $R^* \approx 200$ μm, but with the expected deviation at the smaller

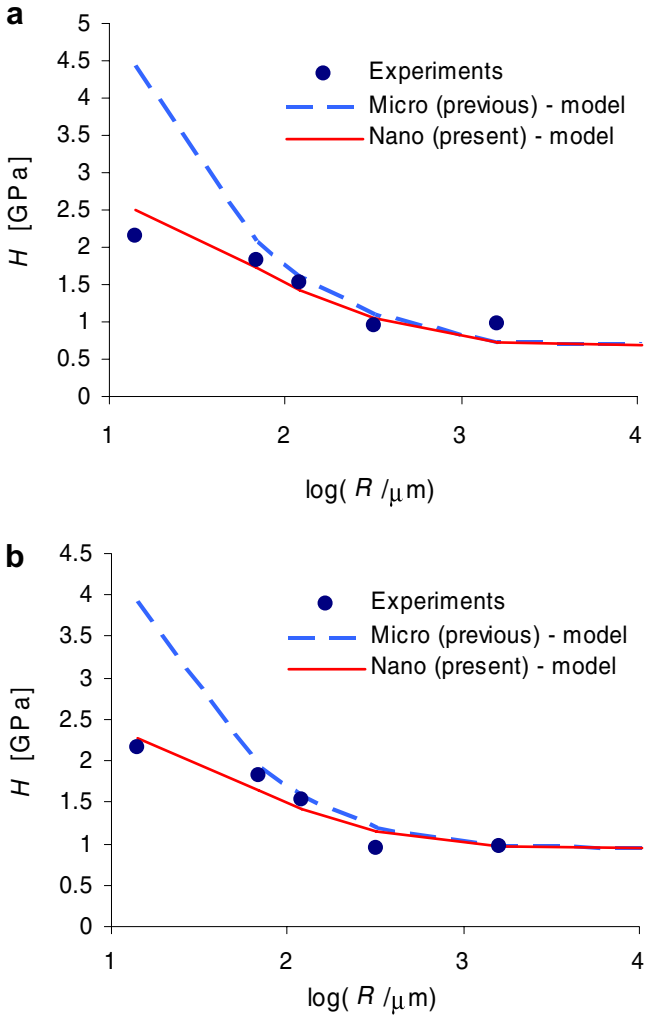

Fig. 3. Comparison between "micro-models" [4,6] and the present "nano-model" fitted to experiments on spherical indentation [6]. Two different sets of parameters are considered: (a) $H_{\text{macro}} \approx 0.9$ GPa, $R^* \approx 250$ μm (dotted line) that, introduced into the nano-model (solid line) with $H_{\text{nano}} \approx 3$ GPa, result in a closer agreement with experiment (points); (b) the same, but for $H_{\text{macro}} \approx 0.6$ GPa, $R^* \approx 750$ μm (dotted line), or, in addition, $H_{\text{nano}} \approx 5$ GPa (solid line). Note the difference in the model predictions at the smaller size scales.

size-scales as predicted by our model, and fitted with $H_{\text{nano}} \approx 2$ GPa. The same material, but in a cold-worked state, was similarly investigated, giving $H_{\text{macro}} \approx 0.9$ GPa and $R^* \approx 3.6$ μm, with a deviation described by our model considering the finite value $H_{\text{nano}} \approx 2$ GPa.

Furthermore, we note that at the true atomic scale we expect even higher values for H_{nano} than deducible from larger-scale experiments, i.e., as anticipated, the hardness upper bound would become the theoretical material value H_{theo}. This behaviour would be described by Eq. (6) considering the formal substitution $H_{\text{nano}} \to H_{\text{theo}}$; thus, a nano-scaling could take place. Such a nanoscaling has been experimentally observed in the indentation hardness of surface Si(1 1 1) films with an indentation depth as small as 1 nm [17]. The hardness for an indentation depth of 2.5 nm was 16.6 GPa and dropped to 11.7 GPa at a depth

of 7 nm, from which we deduce a slope of −0.34, thus suggesting $H_{\text{theo}} \gg 16.6$ GPa.

4. A general spatial–temporal scaling law

Our treatment can further be generalized. For a given nominally constant property P, the generalization of Eq. (6) is straightforward:

$$\frac{P(S/V)}{P_{\text{nano}}} = \left(\frac{(P_{\text{nano}}/P_{\text{macro}})^{\zeta} - 1}{\ell S/V + 1} + 1 \right)^{-1/\zeta} \tag{10}$$

in which the parameter ζ has to be introduced, since a material property could also, for example, be $P = H^2$ (for which $\zeta = 1$, to match Eq. (6)) or $P = H^{-1} (\zeta = -2)$, or others. The asymptote at P_{macro} is classical and intrinsic in considering a nominally constant property, whereas that at P_{nano} appears as a consequence of the existence of a nanoscale quantization. The law of Eq. (10) can be applied for predicting the scaling of a given property, starting from the surface-to-volume ratio of the domain in which the energy exchange or flux, not necessarily a dissipation, occurs.

For a signal (e.g., a wave) propagating at constant velocity, the size-scale R is connected to the time-scale t by $R \propto t$; in this context Eq. (10) is similarly rewritten as ($S/V \propto 1/R \propto 1/t$):

$$\frac{P(t)}{P_{\text{fast}}} = \left(\frac{(P_{\text{fast}}/P_{\text{slow}})^{\xi} - 1}{\tau/t + 1} + 1 \right)^{-1/\xi} \tag{11}$$

where τ is a characteristic time and ξ is a constant. Eq. (11) correlates fast and slow dynamics. To combine Eqs. (10) and (11), two complementary ways can be followed: inserting Eq. (10) into Eq. (11) (i.e., considering P_{nano} and P_{macro} in Eq. (10) as a function of time and of $P_{\underset{\text{fast}}{\text{nano}}}$, $P_{\underset{\text{slow}}{\text{nano}}}$, $P_{\underset{\text{fast}}{\text{macro}}}$, $P_{\underset{\text{slow}}{\text{macro}}}$ according to Eq. (11)), or vice versa (considering P_{fast} and P_{slow} in Eq. (11) as a function of the surface-to-volume ratio and of $P_{\underset{\text{nano}}{\text{fast}}}$, $P_{\underset{\text{nano}}{\text{slow}}}$, $P_{\underset{\text{macro}}{\text{fast}}}$, $P_{\underset{\text{macro}}{\text{slow}}}$ according to Eq.(10)); note that $P_{\underset{\text{nano}}{\text{fast}}} \equiv P_{\underset{\text{fast}}{\text{nano}}}$ and so on, thus, synthetically, the condition of symmetry $P_{\text{ab}} \equiv P_{\text{ba}}$ holds. Following the two complementary approaches, we find the same result only if the self-consistent conditions $\delta = P_{\underset{\text{nano}}{\text{slow}}}/P_{\underset{\text{macro}}{\text{slow}}} = P_{\underset{\text{nano}}{\text{fast}}}/P_{\underset{\text{macro}}{\text{fast}}}$ are valid, i.e., synthetically, for $P_{\text{ab}}/P_{\text{ac}} = P_{\text{db}}/P_{\text{dc}} \equiv P_{\text{b}}/P_{\text{c}}$. Thus, we can formulate a self-consistent general spatial–temporal scaling law in the following form:

$$\frac{P(S/V,t)}{P_{\underset{\text{fast}}{\text{nano}}}} = \left(\frac{(P_{\text{nano}}/P_{\text{macro}})^{\zeta} - 1}{\ell S/V + 1} + 1 \right)^{-1/\zeta} \times \left(\frac{(P_{\text{fast}}/P_{\text{slow}})^{\xi} - 1}{\tau/t + 1} + 1 \right)^{-1/\xi}, \quad P_{\text{ab}}/P_{\text{ac}} = P_{\text{b}}/P_{\text{c}}.$$

5. Example of applications

The generality of the formulation suggests to us that the law of Eq. (6) could have many applications. One example is in the design of syringes of different diameter D penetrating a ductile material (such as a biological soft tissue), for which the force is predicted to be $F_{\text{syringe}} \approx \pi D s H(D)$, where D is the syringe diameter and s is its thickness; accordingly, the maximum length to avoid elastic instability of the syringe will be $l_{\max}(D) \approx \pi \sqrt{EI/F_{\text{syringe}}(D)} \approx \frac{\pi D}{\sqrt{8}} \sqrt{E/H(D)}$, where E is the Young's modulus and I is the moment of inertia of the syringe: thus, the hardness scaling implies a deviation from linearity (between $l_{\max}$ and D). Considering, for example, a single-walled carbon nanotube and the following reasonable parameters $D = 10$ nm, $s = 0.34$ nm (interwall carbon spacing), $H(D) \approx H_{\text{nano}} = 10$ GPa, $E = 1$ TPa, would result in the following plausible estimations $F_{\underset{\text{syringe}}{\text{nano}}} \approx 107$ nN and $l_{\max} \approx 111$ nm.

An additional example is on the design of bullet-proof jackets as a function of the projectile diameter D and kinetic energy K: the work needed to penetrate into the material for a length l is $W(D) = \int_0^l A(h,D)H(h,D)\,\mathrm{d}h = l\langle A(D)H(D)\rangle$, where $A(D) = \pi D^2/4$ is the cross-section bullet projected area; since W must be equal to the bullet kinetic energy K, its minimum thickness l is predicted to be $l_{\min}(D) = K/\langle A(D)H(D)\rangle$. For example, considering a bullet mass of 100 g, velocity of 1 km s^{-1}, $A = 1$ cm^2 and $H = 10$ GPa, would correspond to a plausible value of $l_{\min} \approx 5$ cm.

Defining the impact strength as the energy was spent over the removed volume, the last example shows that such a parameter is for plastic materials of the order of their hardness, but note, at the investigated size-scale (and $H_{\text{nano}} \gg H_{\text{macro}}$). A similar result is found for brittle materials at the macroscale, where the impact strength is of the order of the material macro-strength [18]: thus, our argument suggests its validity at all size scales. That is, for plastic materials the impact strength is of the order of their hardness whereas for brittle materials it is of the order of their material strength, but at the considered size scale. This finding, if confirmed, could have interesting applications also in impact or explosion and tribological studies, from the nano- to the mega-scale.

For material strength $P = \sigma, \zeta = 2$ in Eq. (10) (as for H) and considering self-similar structures, i.e., $V/S \propto R$, as the characteristic structural size (but note that in general Eq. (10) describes also the shape effects), we deduce

$$\sigma_{\text{R}} = \sigma_{\text{macro}} \sqrt{1 + \frac{\ell^*}{R + \ell'}}$$

with $\ell^* = (1 - \delta^{-2})\ell$, $\ell' = \delta^{-2}\ell$ and $\delta = \sigma_{\text{nano}}/\sigma_{\text{macro}}$ (smaller is stronger). This is a scaling law taking into account the quantization of the energy flux and for $\delta \to \infty$ agrees with Carpinteri's law [15]; such a law has already been demonstrated to agree with microtorsion [19] and microbending [20] experiments, see Refs. [21,22].

The law of Eq. (10) can also be applied to complex and chaotic systems, where the multiscale energy flux arises in a fractal domain of positive dimension D (usually comprised between 2 and 3, i.e., the fractal surface of the energy flux is usually comprised between a Euclidean surface and volume); in this case, $S \propto V^{D/3}$ [18,23], no matter if we are considering fractal fragments or dislocations, thus brittle or plastic materials. Accordingly, $S/V \propto R^{D-3}$ in Eq. (10) with R structural size. For example, for a hierarchical material (as for bone, nacre and dentine) we derive $D = 3\ln n/\ln(n/\varphi)$, where $n > 1$ and $0 < \varphi < 1$ are the number and volumetric fraction content of sub-inclusions in a main inclusion (the demonstration is left up to the reader). One example is given by the scaling of the energy density $P = \psi$ (nominally a material constant) during fragmentation of solids, for which $\zeta = 1$ (since $\psi \propto \sigma^2$), in agreement at intermediate size scales with the mesoscopic scaling $\psi \propto S/V \propto R^{D-3}$ [18,23]. Interestingly, such a law is also extensively applied for describing the scaling of the energy per unit mass spent by biological systems on growth [23–25], thus, Eq. (10) straightforwardly extends this biological scaling law, as well as the large number of allometric biological laws [25] that can be derived from it.

An example of an application of Eq. (11) is on the variability of dynamic strength $P = \sigma$ ($\xi = 2$, from dynamic fracture mechanics) as a function of the time to failure t. The impact strength (σ_{fast}) is observed for the majority of the systems to be approximately twice the static strength (σ_{slow}); this seems to be related to the existence of an incubation time (τ) for fracture nucleation, of the order of the time needed to generate a fracture quantum and thus again related to a quantization [26]. It is evident that Eq. (11) with $\sigma_{\text{fast}} \approx 2\sigma_{\text{slow}}$ captures the related transition.

For complex and chaotic fractal systems, the result previously reported ($S/V \propto R^{D-3}$) is formally traduced in Eq. (11) as $\tau \propto t^{D-2}$, where D is here connected to the fractal dimension of the time distributions.

6. Conclusions

In this paper we have derived a general size/shape-effect law for nanoindentation, based only on the surface-to-volume ratio of the domain in which the energy flux occurs, considering different sizes and shapes of the indenter. The law matches as limit cases all the well-known hardness scaling laws proposed in the literature, but also explains their deviations as experimentally observed towards the nanoscale. Its applicability is demonstrated for conical, spherical and flat indenters; experimental comparison confirms the key role played by the peculiarity of this model, i.e., the existence of a bounded hardness or total dislocation density. The limitations of the model have been discussed in depth. A general spatial–temporal scaling law has also been formulated and a few simple examples of applications have been provided in different fields, such as materials science and biology.

Acknowledgements

The author thanks A. Carpinteri for having introduced him to size-effects and Dorothy Hesson for the English grammar supervision. Support by the Italian Ministry of University and Research (MIUR) is gratefully acknowledged.

References

[1] Mott BW. Micro-indentation hardness testing. London: Butterworths; 1956.
[2] Ashby MF. The deformation of plastically non-homogenous materials. Philos Mag 1970;21:399–424.
[3] Nye JF. Some geometric relations in dislocated crystals. Acta Metall 1953;1:153–62.
[4] Nix WD, Gao H. Indentation size effects in crystalline materials: a law for strain gradient plasticity. J Mech Phys Solids 1998;46:411–25.
[5] Poole WJ, Ashby MF, Fleck NA. Micro-hardness tests on annealed and work-hardened copper polycrystals. Scripta Mater 1996;34:559–64.
[6] Swadener JG, George EP, Pharr GM. The correlation of the indentation size effect measured with indenters of various shapes. J Mech Phys Solids 2002;50:681–94.
[7] Lim YY, Chaudhri MM. The effect of the indenter load on the nanohardness of ductile metals: an experimental study on polycrystalline work-hardened and annealed oxygen-free copper. Philos Mag A 1999;79:2879–3000.
[8] Arsenlis A, Parks DM. Crystallographic aspects of geometrically-necessary and statistically-stored dislocation density. Acta Mater 1999;47:1597–611.
[9] Huang Y, Zhang F, Hwang KC, Nix WD, Pharr GM, Feng G. A model of size effects in nano-indentation. J Mech Phys Solids 2006;54:1668–86.
[10] Taylor GI. Plastic strain in metals. J Inst Met 1938;13:307–24.
[11] Wiedersich H. Hardening mechanisms and the theory of deformation. J Met 1964;16:425–30.
[12] Pugno N, Ruoff R. Quantized fracture mechanics. Philos Mag 2004;84/27:2829–45.
[13] Griffith AA. The phenomena of rupture and flow in solids. Phil Trans Roy Soc A 1920;221:163–99.
[14] Tabor D. The hardness of metals. Oxford: Clarendon Press; 1951.
[15] Carpinteri A. Scaling laws and renormalization groups for strength and toughness of disordered materials. Int J Solids Struct 1994;31:291–302.
[16] Oliver WC, Pharr GM. An improved technique for determining hardness and elastic modulus using load and displacement sensing indentation. J Mater Res 1992;7:1564–83.
[17] Bushan B, Koinkar VN. Nanoindentation hardness measurements using atomic force microscopy. Appl Phys Lett 1994;64:1653–5.
[18] Carpinteri A, Pugno N. One-, two- and three-dimensional general laws for fragmentation due to impact and explosion. J Appl Mech 2002;69:854–6.
[19] Fleck NA, Muller GM, Ashby MF, Hutchinson JW. Strain gradient plasticity: theory and experiment. Acta Metall Mater 1994;42:475–87.
[20] Stolken JS, Evans AG. A microbend test method for measuring the plasticity length scale. Acta Mater 1998;46:5109–15.
[21] Gao H, Huang Y, Nix WD. Modeling plasticity at the micrometer scale. Naturwissenschaften 1999;86:507–15.
[22] Gao H, Huang Y, Nix WD, Hutchinson JW. Mechanism based strain gradient plasticity I. Theory J Mech Phys Solids 1999;47:1239–63.
[23] Carpinteri A, Pugno N. Are the scaling laws on strength of solids related to mechanics or to geometry? Nat Mat 2005;4(June):421–3.

[24] Guiot C, Delsanto PP, Carpinteri A, Pugno N, Mansury Y, Deisboeck TS. The dynamic evolution of the power exponent in a universal growth model of tumors. J Theor Biol 2006;240: 459–63.

[25] West GB, Brown JH. Life's universal scaling laws. Phys Today 2004;57:36–43.

[26] Pugno N. Dynamic quantized fracture mechanics. Int J Fracture 2006;140:158–68.